Journal of Civil Structural Health Monitoring (2024) 14:209–221
https://doi.org/10.1007/s13349-023-00731-3

ORIGINAL PAPER

Automatic detection of delamination on tunnel lining surfaces from laser 3D point cloud data by 3D features and a support vector machine

Tsukasa Mizutani[1] · Takahiro Yamaguchi[1] · Kazutomo Yamamoto[2] · Tetsuya Ishida[3] · Yoshifumi Nagata[4] · Hinari Kawamura[5] · Tomoaki Tokuno[5] · Kiyoshi Suzuki[2] · Yuya Yamaguchi[2]

Received: 25 December 2022 / Accepted: 5 October 2023 / Published online: 28 October 2023

Abstract
A completely automatic algorithm for accurately detecting delamination on tunnel concrete lining surfaces using laser 3D point cloud data is first proposed to facilitate tunnel lining inspection. A mobile mapping system (MMS), which mounts laser sensors and a positioning system, is utilized to measure the geometries of the surfaces at high speed. The algorithm consists of two steps: extraction of the 3D shapes of anomalies and discrimination of delamination from appendages by a support vector machine (SVM). The article focusses on the second step. On tunnel linings, there are many conspicuous appendages such as cables, lights, signs, and water guides which mask the features of delamination. In this study, straightness, a novel 3D feature, is introduced to realize accurate discrimination. An automatic algorithm based on the SVM is developed and validated using real tunnel data, showing an accurate delamination map.

Keywords Mobile mapping system · Delamination · Tunnel linings · Laser 3D point cloud data · Support vector machine

1 Introduction

Aging infrastructures are an important world-wide social problem [1]. Especially, the peelings of tunnel concrete linings are critical because they threaten the safety of road users [2, 3]. To prevent severe accidents, road administrators must detect delamination before it advances to peelings. To maintain the enormous amounts of infrastructure stocks, automatic and high-speed monitoring techniques are indispensable.

In practice, the delamination of concrete structure surfaces is detected by a hammering test. However, it is labor intensive and subjective. Covering large areas of the tunnel lining surfaces by manual inspection is not feasible. Furthermore, it requires skilled inspectors to accurately detect damage. The infrared (IR) camera method detects delamination based on differences in surface temperature [4]. The difference of temperature between day and night are needed for the method to work. An automatic sounding system records acoustic signals [5]. A laser-sounding system hits a light beam to evaluate the dynamic characteristics of delaminated concrete surfaces [6]. A non-destructive monitoring method has been developed inside concrete structures using neuron sources [7]. These methods require special instruments,

✉ Takahiro Yamaguchi
tyamag@iis.u-tokyo.ac.jp

Tsukasa Mizutani
mizu-t@iis.u-tokyo.ac.jp

Kazutomo Yamamoto
kazutomo-yamamoto@aeroasahi.co.jp

Tetsuya Ishida
tetsuya.ishida@civil.t.u-tokyo.ac.jp

1 Institute of Industrial Science, The University of Tokyo, 4-6-1, Komaba, Meguro-ku, Tokyo 153-8505, Japan

2 Aero Asahi Corporation, 3-14-4, Minamidai, Kawagoe, Saitama 350-1165, Japan

3 Department of Civil Engineering, The University of Tokyo, 7-3-1, Hongo, Bunkyo-ku, Tokyo 113-8654, Japan

4 Metropolitan Expressway Company Limited, 1-4-1, Kasumigaseki, Chiyoda-ku, Tokyo 100-8930, Japan

5 Shutoko Engineering Company Limited, 3-10-11, Toranomon, Minato-ku, Tokyo 105-0001, Japan

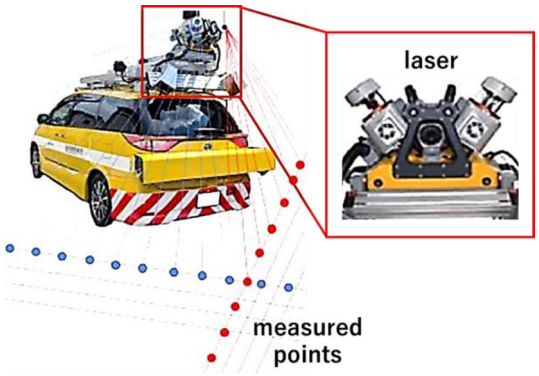

Fig. 1 Mobile mapping system (MMS) for obtaining laser 3D point cloud data

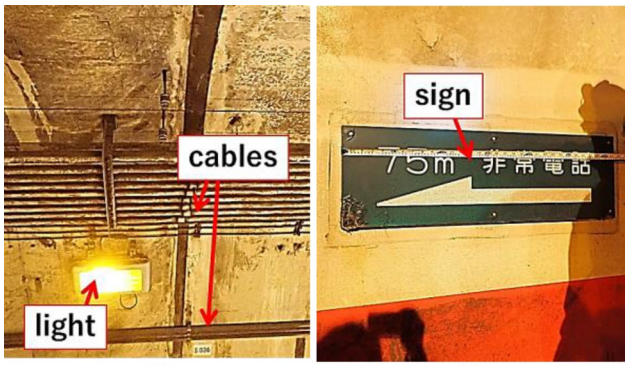

Fig. 2 Appendages on real tunnel linings. **a** Cables and light. **b** Sign

inspection time, and cost. Typical frequency ranges of ground-penetrating radar (GPR) systems are not amenable to thin millimeter-order thickness cracks [8].

The addressed problem of this research is to propose an automatic algorithm for detecting delamination on tunnel concrete lining surfaces using laser 3D point cloud data, aiming to facilitate tunnel lining inspection. A mobile mapping system (MMS) is used here. Ranging lasers and a GNSS/IMU positioning system are mounted on an ordinary MMS (Fig. 1, [9]). The advantage of the MMS is the high-resolution grid data of the height (altitude) of an infrastructure surface is obtained at a high speed.

Previous studies on the laser method are introduced here. Kim et al. estimated spalling areas on precast concrete surfaces using the proposed edge detection algorithm [10]. Yoon et al. illustrated utility cables on tunnel concrete lining surfaces using laser data in a feasibility study [11]. The two research works proposed their own fixed laser scanner system and vehicle-equipped type laser scanner, respectively. They achieved millimeter-order accuracies for assessing each target object. Our group first proposed an automatic algorithm for detecting delamination on tunnel concrete lining surfaces by adopting the-state-of-the-art signal and image-processing algorithms [12, 13]. The areas and maximum height of the delamination were estimated, realizing the quantitative evaluation of damages, and showing their shapes on a 3D map. As reported in our previous research, when delamination advances to a certain extent, which is our target delamination, it causes deformations of at least a several-centimeter area and several-millimeter height. Delamination was detected as a positive peak of local displacements from laser 3D point cloud data.

The problem of the research is that the environment of a real tunnel lining surface is complicated including many conspicuous appendages such as cables, lights, and signs as shown in Fig. 2. Yamaguchi et al. proposed primitive judging criteria based on maximum height and projected areas of 3D anomalies [13]. There are at most several areas of delamination in a 100 m section. Delamination is subtle in natures, resulting in an unacceptable number of false detection cases. It is necessary to increase the accuracy by reorganizing and adding feature values to effectively discriminate artificial objects of appendages from delamination.

Another problem is that there were five thresholds for distinguishing delamination from appendages. The thresholds were arbitrarily selected, which may not be optimized, and not apply to other tunnels. Deep learning algorithms are possible answers, although a large amount of training data with at least ten thousand to one hundred thousand cases is needed to develop a reliable algorithm [14–16]. The automatic construction of classification criteria for sets of high-dimensional vectors composing of feature values using a simple machine-learning algorithm is required. A support vector machine (SVM) is one of the most typical machine-learning algorithms suitable for this type of problem [17–19]. It automatically estimates the optimized division plane in a feature space by maximizing the distances between the plane and vectors. Only vectors which are close to the dividing plane contribute to the construction of the plane. The vectors are called support vectors.

In response to the discussions above, the two contributions of this study are listed below.

1. A novel feature, ‘straightness’ of an outline of a 3D object is defined based on Hough transform. The feature and maximum height, area, and occupancy are used to eliminate artificial objects of tunnel appendages. Straightness is a novel index in the context of pattern analysis and image-processing fields.
2. After constructing high-dimensional feature vectors for inputs, an SVM is trained and validated using real tunnel laser measurement data to realize the automatic detection of delamination.

The implementation of an SVM is important for realizing the automatic detection of delamination. The effectivity of the novel feature is quantitatively discussed in the automatic detection by SVM section. The rest of this study is organized as follows: the proposed algorithm section introduces the concept of the algorithm of the previous research and proposal of this research; the measurement system and data configuration and evaluation metrics sections describe the configuration of the utilized system, training and validation data; the proposed 3D features section proposes novel 3D features for automatic detection; the automatic detection by SVM section presents the detection results by the developed SVM. Parametric studies were also conducted to optimize the SVM and demonstrate the effectiveness of the proposed features; the discussions and conclusions sections summarize the findings of the research to conclude the article.

2 Proposed algorithm

The entire concept of the algorithm is summarized in Fig. 3 by the flow chart. Figure 4 depicts calculation steps 1.1–1.4. The concepts of the steps 1.1–1.4 are explained in [10, 11]. The profiles of tunnels such as cross sections and inclinations are meter-order in sizes in horizontal and height directions. Appendages are centimeter-order. Delamination is centimeter-order in the area and millimeter-order in the height. To detect small delamination, the profiles were removed from the raw data. The travel (longitudinal) direction is the running direction; the circumferential (lane width) direction is the transverse direction along the circle of a tunnel. The height (altitude) direction is the normal direction to the horizontal plane (travel–circumferential) plane. In the travel and circumferential directions, the profiles were estimated by time-series analysis updated by a Kalman filter (step 1.1, [20]).

Hilbert transform was applied to each measurement line to draw an envelope (step 1.2, [21, 22]). Anomaly peaks were detected by the differences between the data and envelopes. The threshold was set 5 mm [10, 11]. The algorithm considers peeling and other types of damages. In this study, only positive peaks were extracted to target delamination. Reference lines were estimated by detecting the change points and extrema. To evaluate areas, the detected sections were overplotted on a 2D map (step 1.3). Morphology transform was applied to accurately detect anomaly areas by smoothing boundaries and removing small noise [23, 24]. Reference lines were approximated by reference planes to extract 3D shapes of anomalies (step 1.4).

Figure 4a shows raw tunnel data. The curved surface corresponds to the tunnel ceiling. The profiles, particularly the cross sections of the tunnels, are dominant in the tunnel laser data. Figure 4b displays a map after subtracting the

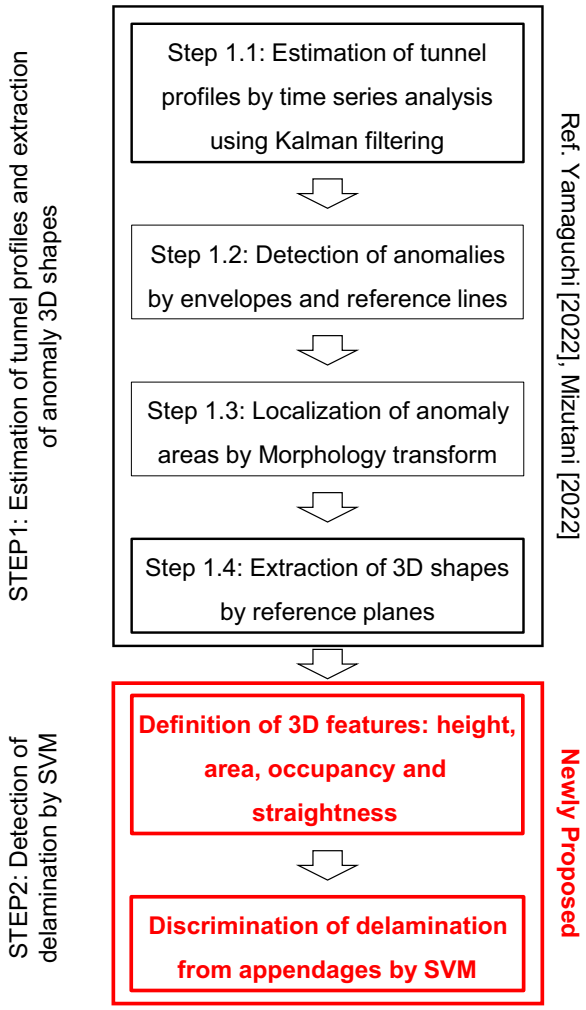

Fig. 3 Flowchart. The algorithm is based on Mizutani et al. (2022), Yamaguchi et al. (2022). This research discusses the extraction of 3D features and automatic detection of delamination by an SVM

estimated profiles from the raw data. Peaks which are corresponding to the anomalies are observed. The peaks of the cables continued in the travel direction, whereas the lights are represented by local displacements. Even at this step, delamination is not evident because of the prominent peaks of the appendages. Figure 4c exhibits the circumscribed rectangles of all the detected anomalies after the Hilbert and morphology transforms. All the features are observed including the cables, lights, signs, water guides, and target delamination.

Subsequently, 3D features are calculated for the extracted anomalies. Delamination is discriminated from the appendages by setting thresholds on the feature values. The proposal of this study is related to this step. In addition to the maximum height, area, and occupancy, straightness is newly introduced to eliminate artificial objects. A classification algorithm based on an SVM is developed to automate the

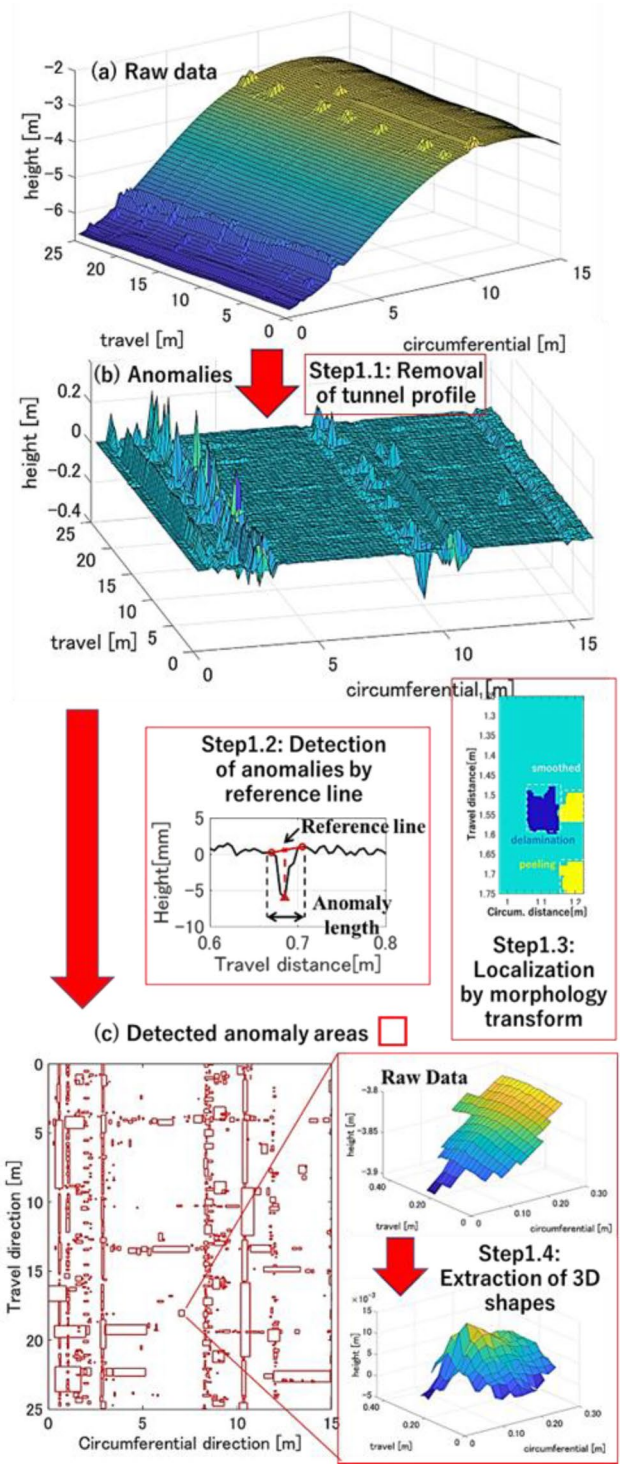

Fig. 4 Extraction of 3D shapes of anomalies from laser measurement data. **a** Raw tunnel lining data. **b** After removal of a tunnel profile. **c** Anomaly areas and extracted 3D shapes. Corresponding steps 1.1–1.4 in Fig. 3 are shown here

detection process. The detected delamination is displayed on a 2D delamination map and a 3D quarter-view map with its 3D shape.

Table 1 Accuracy of laser measurement system

Parameter	Nominal value
1σ variation of the measured distance in the height direction at 25 m	0.4 mm
Measurement speed	1 million points/s
Sensor rotation speed	200 Hz
GNSS/IMU positioning resolution	0.02–0.05 m

3 Measurement system

The measurement system is shown in Fig. 1. A laser sensor radiates light beams at each vehicle position and scanning angle. The system uses two laser sensors to accelerate the measurements. It needs certain time for laser sensors to scan assigned areas. By utilizing the two sensors simultaneously, the scanning time can be halved. This point is important for maintaining a vehicle speed.

The electric signals are converted to optical signals using a laser diode (LD). The distances between the sensors and target objects are measured considering the phase delays of the transmitted and received sinusoidal waves of the lights. Further details are beyond the scope of this study.

The measured distances, referred to as 3D point cloud data, are converted to grid height data by referring to the GNSS/IMU positioning system. Table 1 summarizes the configuration of the laser measurement system. The variation of the measured distance in the height direction is 0.4 mm, small enough to measure millimeter-order deformations. The most important measurement parameters are the resolution of the grid data and the corresponding speed of the vehicle. The research adopts a resolution of 2 cm. The MMS scans the surfaces of tunnels at approximately 10–20 km/h to achieve a resolution of 2 cm. Further increasing the speed, e.g., at 50–60 km/h, the corresponding resolution is about 5 cm. However, coarse data are not favorable for the accurate detection of delamination.

4 Data configuration and evaluation metrics

4.1 Preparation of training data

Table 2 summarizes the manual inspection target tunnels and the corresponding laser measurement data used in the research. Three tunnels No. 1–No. 3 consisting of five sections data No. 1–No. 5 were measured and inspected. Sections No. 1–3 are in the same tunnel. The locations vary around the capital area of Tokyo, Japan. Tunnel No. 3 is 200 km distant from the other tunnels. The construction methods and years are also varied to demonstrate the applicability of the algorithm to other tunnel data. Sheet piling

Table 2 Manual inspection target tunnels and laser data for training and validation of SVM

Tunnel	No.	Data	Location (in Japan)	Construction method	year	Section length (travel by circum.)	No. of delam.
Tunnel 1	No. 1	Validation	Nagano pref	Sheet piling	1975	20 m by 15 m	6
	No. 2	Training				25 m by 12 m	6
	No. 3					25 m by 15 m	2
Tunnel 2	No. 4		Nagano pref	NATM	1991	22 m by 12 m	0
Tunnel 3	No. 5		Kanagawa pref	Sheet piling	1963	60 m by 12 m	2

and new Austrian tunneling method (NATM) are the typical tunnel construction methods. The tunnels are 30–60 years old.

Manual inspection was performed; the total number of the detected delamination was 16. Delamination was not detected in the area of the data No. 4. Therefore, only the appendages were extracted. The other tunnels included multiple areas of delamination, which necessitated dense condition monitoring. As an example, Fig. 5 shows the inspection results of the data No. 1. Step-like deformations and delamination caused by the free lime were reported.

The laser data contain longer sections. To match the areas of the manual inspection results with the laser data, appendages were utilized. Frequency analysis was applied to emphasize features of 20–30 cm scale sizes following the previous research [25]. The areas of the delamination detected by the manual inspectors were located by referring to the characteristic features such as the cables and lights (Fig. 5a).

Then, the step 1 of Fig. 3 was applied to the laser data to extract the 3D shapes of the features. As shown in the red rectangles in Fig. 4c, all the features including delamination and appendages were extracted. Referring to the delamination areas, each feature was labeled as a delamination or appendage. The SVM parameters were trained using the data shown in Table 2. The data No. 1 of the tunnel No. 1 were used as validation (test) data. The other four datasets, data No. 2–No. 5 were used for training. To consider the importance of large-area delamination, the feature vectors were replicated in proportion to the areas of delamination. The

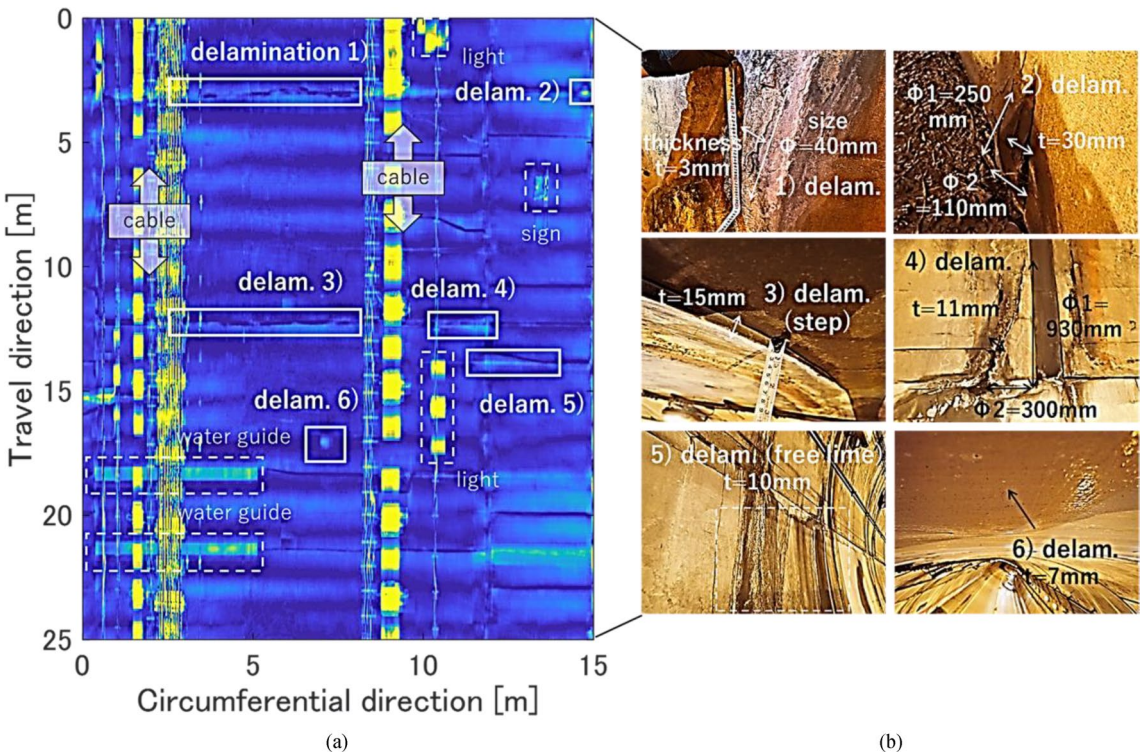

Fig. 5 Delamination of the data No. 1. **a** Frequency analysis of data and delamination areas detected by manual inspection. Yellow areas are the characteristic features emphasized by frequency analysis. **b** Sizes of delamination were measured for references

ratio of the total number of the detected features between the training and validation datasets was approximately 3.4:1. The dataset was arranged to demonstrate the applicability of the developed SVM algorithm to the unforeseen tunnel data.

4.2 Evaluation metrics

Two indices are introduced in this study to evaluate the performance of the trained SVM. Accuracy is the ratio of the number of correctly classified data among validation data. Because the number and areas of the appendages are larger than the delamination, the data is not balanced between the two categories. Therefore, the area under the curve (AUC) of a precision–recall (PR) curve is also compared. Accuracy and AUC show similar tendency. However, they do not necessarily correspond to each other one to one [26].

The delamination and quarter-view maps were plotted for the data No. 1 to demonstrate the performance of the algorithm. The ratio of the numbers of the successfully detected areas of the delamination among the true delamination, detection rate, and ratio of the areas of the true delamination among the detected areas, precision, were also evaluated as will be discussed in the detection results section.

Because of the complicated geometries of the delamination and nature of the manual detection, there may be a slight difference between the estimated shapes of delamination and inspection results. In the previous research, the estimation error of the areas and heights was within 20% [10]. The detailed comparison between the estimated and measured shapes of the delamination is not the target of the research. The successful detection by the SVM indicates the validity of the estimation algorithm.

5 Proposed 3D features

Figure 6a shows a delamination case. The maximum heights and areas of the features were calculated. These two features contain information on their scales. The heights and areas of the appendages are larger than delamination. Furthermore, too small features can be considered as noise and ignored. Figure 6b shows the occupancy of the feature. The features were projected onto three planes, horizontal, circumference–height, and travel–height planes. Circumscribed rectangles were drawn for projected areas. Occupancy is the ratio between the area of the rectangle and projected feature. The concept of occupancy is to simply evaluate the shapes of 3D features in the three planes.

Straightness is a novel index, which is proposed in this study. The profiles of the artificial objects are composed of straight lines, whereas the delamination has a complicated profile. Figure 7 explains the process of evaluating straightness. Figure 7a displays the area of

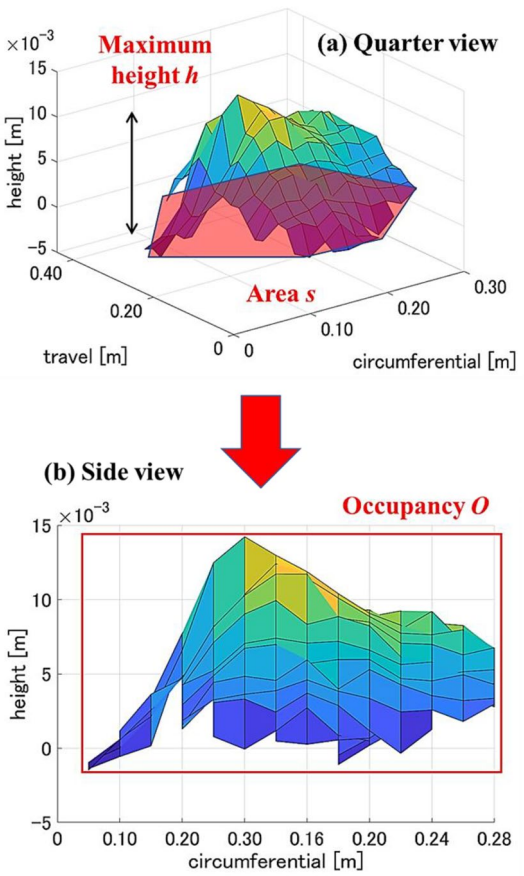

Fig. 6 Extraction of 3D features. **a** Quarter view. **b** Side view. The maximum height, area and occupancy were defined. Three occupancy values were calculated from a top and two side views

the delamination shown in Fig. 6 with the corresponding height in a colormap. Figure 7b shows the profile of the area. Area projections can be considered in the horizontal, circumference–height, and travel–height planes. Therefore, three straightness values were obtained in the three planes. Figure 7c shows the Hough transform of the profile shown in Fig. 7b. The number of the passing lines for each pixel is the parameter of the Hough transform. The numbers were counted for each pixel of the profile. Yellow areas in the Hough space indicate large numbers. Profile images which are too coarse, for example, only several pixels by several pixels, may fail to extract peaks in the Hough space. Therefore, the images were up-sampled 10 times on both axes. In the Hough space of Fig. 7c, each peak of a yellow area corresponds to a straight line. The longer the lines were in the image, the higher the peaks were in the Hough space.

In the Hough space, the n highest peaks were extracted; $n = 5$ was adopted to target the squared features of the appendages, such as cables and lights. The summation I of the peak values p_k of the n peaks was calculated.

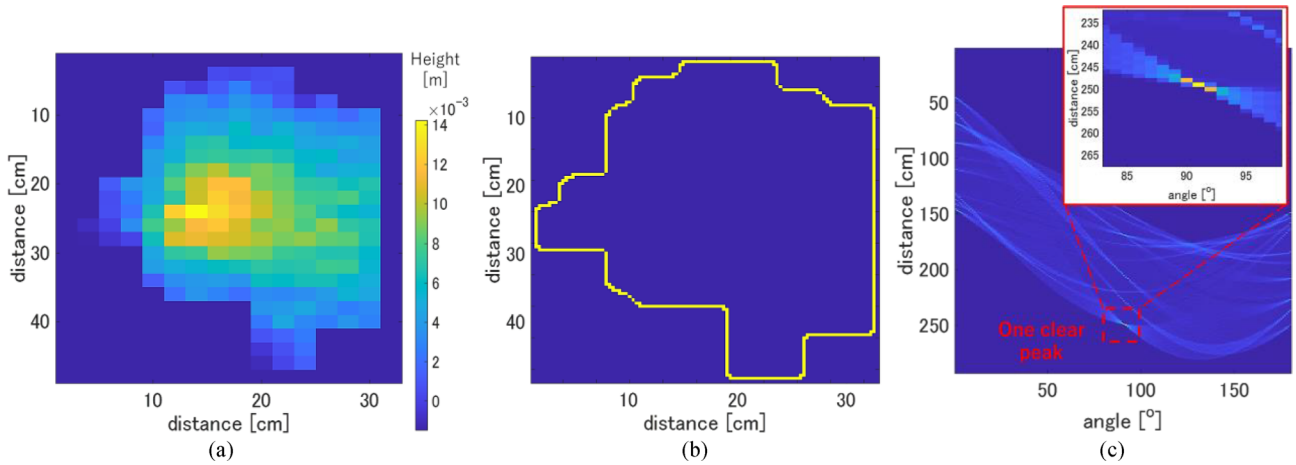

Fig. 7 Extraction of straightness. **a** Area of the delamination of Fig. 8. Colors represent the height. **b** Profile of the feature. Profile image is 10 times up-sampled. **c** Hough transform of the profile. Colors are the number of passing lines, a parameter of the Hough transform for line detection. One clear peak is observed to contribute to the straightness value in this case

$$I = \sum_{k=1}^{n} p_k. \tag{1}$$

The ratio between I and the total number of the pixels in the profile L was defined as the straightness S to remove the effect of the scales of the features.

$$S = I/L. \tag{2}$$

The longer the selected five lines were in the profile, the larger the summation I was; Given the same profile length L, S should be larger from Eq. (2). n is the parameter. An excessively small and large n will fail to delineate lines. n was not sensitive to the detection results, possibly because the relationship of S was important in SVM, and polygons with many edges may not exist in the data. As shown in Fig. 7c, a clear peak was observed to contribute the S value.

Figure 8 shows examples of a circle and square to explain the characteristics of straightness. From Fig. 8a, S of the square is approximately 1.1. When all pixels in a profile belong to one of the n lines, one pixel increases the peak value by one, consequently $S \cong 1.0$. Theoretically, for polygons with several edges smaller than or equal to n, $S = 1$. Owing to the effects of the intersections of the edges and limited resolution of the images, the calculated S was slightly larger than 1.0. Figure 8b shows a polygon with an infinite number of edges, that is, a circle, indicating $S = 0.3$. S of any profile lies between the polygon and circle. S of a complicated winding and jaggy profile is small, and profile composed of several straight lines is large. In the case of delamination in Figs. 6 and 7, $S = 0.5$. The profile was close to a circle and far from artificial objects.

One of the most important characteristics of a feature value is scale invariance. Straightness and other features exhibit scale invariance. Straightness also exhibits rotation invariance. However, occupancy does not hold for rotation invariance. The successful detection results indicated that most of the analyzed appendages are aligned along the travel or circumferential directions, for example, the cables. An SVM may automatically construct rotation-invariant features by combining the feature values.

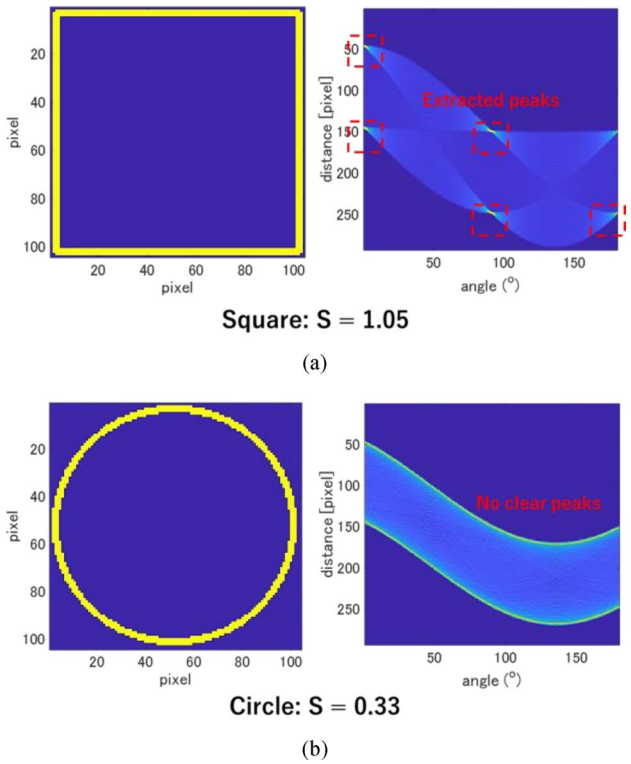

Fig. 8 Examples of the straightness values of the profiles. **a** Square. **b** Circle. Left figures are profiles and right are Hough transforms. Corresponding straightness values are shown

The area and maximum height of a feature are related to its scale. Occupancy is related to the geometry of a feature area. The 3D geometries were evaluated by considering the three planes. However, the problem is that polygons with the same areas within circumscribed rectangles will show the same occupancy. Straightness is related to the geometry of the feature profile. Considering all the features, 3D shapes are precisely evaluated.

Summarizing the discussions, the features about scales, maximum height h and area s, features about the geometries of areas, occupancy in the three planes O_{yz}, O_{zx}, O_{xy}, features about the geometries of profiles, straightness in the three planes S_{yz}, S_{zx}, S_{xy}, total four features with eight parameters were introduced. An integrated feature vector F is defined as follows:

$$F = \left(h, s, O_{yz}, O_{zx}, O_{xy}, S_{yz}, S_{zx}, S_{xy}\right). \tag{3}$$

Using the feature vectors as an input to an SVM, a machine-learning model is trained to automatically construct classification criteria between the delamination and appendages.

Each type of an object shows characteristic feature values. Figure 9 introduces the examples of extracted features. Figure 9a–d corresponds to delamination, cable, light, and water guide, respectively. As shown in Fig. 9, the cables are narrow rectangles in the horizontal plane and have tall heights; the lights and signs are box-shaped; the water guides and repair patches are U-shaped or box-shaped, depending on adjacent features; the delamination is convex. The occupancy of the cables in the perpendicular direction and boxes was high, whereas that of the U-shaped objects was low. The occupancy of the convex plane was moderate on all projected planes. By setting thresholds for higher and lower occupancy, the delamination was detected reducing the false detection of the appendages.

The heights of the cables and lights were 15–20 cm in Fig. 9, which was higher than those of the delamination and water guide, 1–2 cm. The occupancy O_{yz} of the cable was low and the light was high. The occupancy of the water guide in one direction (O_{xy}) was low, whereas in the other directions they were high. The straightness S_{yz} of artificial objects, such as cables, lights, and water guides, is generally high. In the case of the crossing cables shown in Fig. 9b, S_{yz} was low, whereas O_{yz} was high. All parameters were moderate in the case of the delamination, indicating a convex 3D volume. From Fig. 9, the features were effectively defined to distinguish the delamination from the artificial objects.

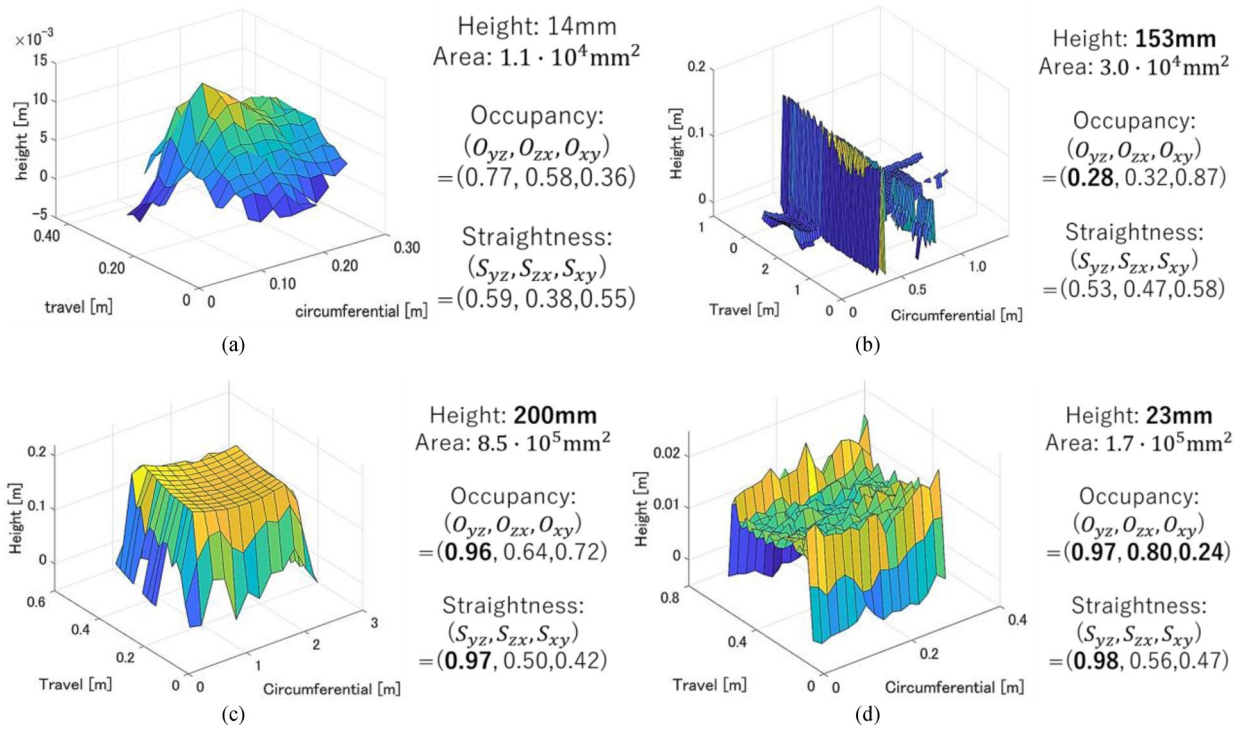

Fig. 9 Extracted typical 3D shapes and feature values. **a** Delamination. **b** Cables. **c** Light. **d** Water guide. Yellow and blue areas show high and low heights respectively. All the target parameters, height, area, occupancy, and straightness are shown

6 Automatic detection by SVM

6.1 Detection results

Figure 10 shows the detection result of the data No.1 by the optimized SVM, the manual inspection result of which is shown in Fig. 5. Figure 10a shows the detected areas of the delamination, which is distinguished from the other features shown in Fig. 4c. Figure 10a indicates that the target delamination Nos. 1 and 3–6 were successfully detected in the appropriate positions compared to Fig. 5a. The detection rate was $5/6 = 83\%$. The total detected area was 22,540 cm^2, while 16,100 cm^2 is the true delamination area. Therefore, of the detected areas, 72% had actual delamination. In the context of deep learning, intersection over union (IoU) is a popular evaluation criterion for matched areas, the typical values of which may be 30–40% in the case of region proposal problems [27–29]. The detection rate 83% and precision 72% were high. Using the proposed SVM algorithm, the possible delamination regions were localized from 3,750,000 cm^2 (25 m by 15 m) to 22,540 cm^2, which was approximately 0.8%. Figure 10b shows a quarter-view of the estimated 3D shapes to visualize the realistic delamination shapes.

Figure 11 shows the areas and 3D map of the appendages which remain after removing the delamination from all the detected features. The features of the cables aligned in the travel direction are apparent. The lights between the cables, sign, and water guides were successfully classified as appendages. These features are useful for locating the positions of delamination during repair works and analyzing the causes of the delamination.

6.2 Parametric study

A kernel function is the important hyper-parameter of the SVM. The kernel function is a nonlinear conversion applied to the input feature vectors, the effect of which is equivalent to drawing nonlinear dividing planes in a feature space. The kernel function improved the performance of the SVM classification. Figure 12 shows a comparison of different kernel functions. Linear is no kernel trick; polynomial is third order. Compared to the ordinally linear SVM, a radial basis function (RBF) kernel increased the area under the curve (AUC) by approximately 0.3, whereas the polynomial function decreased the accuracy and AUC. The most appropriate kernel function depends on the problem. The RBF kernel was adopted in this study.

A feature vector is defined by Eq. (3). To evaluate the effect of these parameters, the performances of SVM models were compared by changing the combinations of the feature values. Table 3 lists the configurations of the SVM models. Model No. 1 (height–area) considers only the scales of the anomalies. Model 2 (previous) is a model of Yamaguchi (2022) [11]. Model 3 (proposed) additionally considers the straightness of the profile on a horizontal plane. Model 4 (all) includes straightness in all three directions. Accuracy

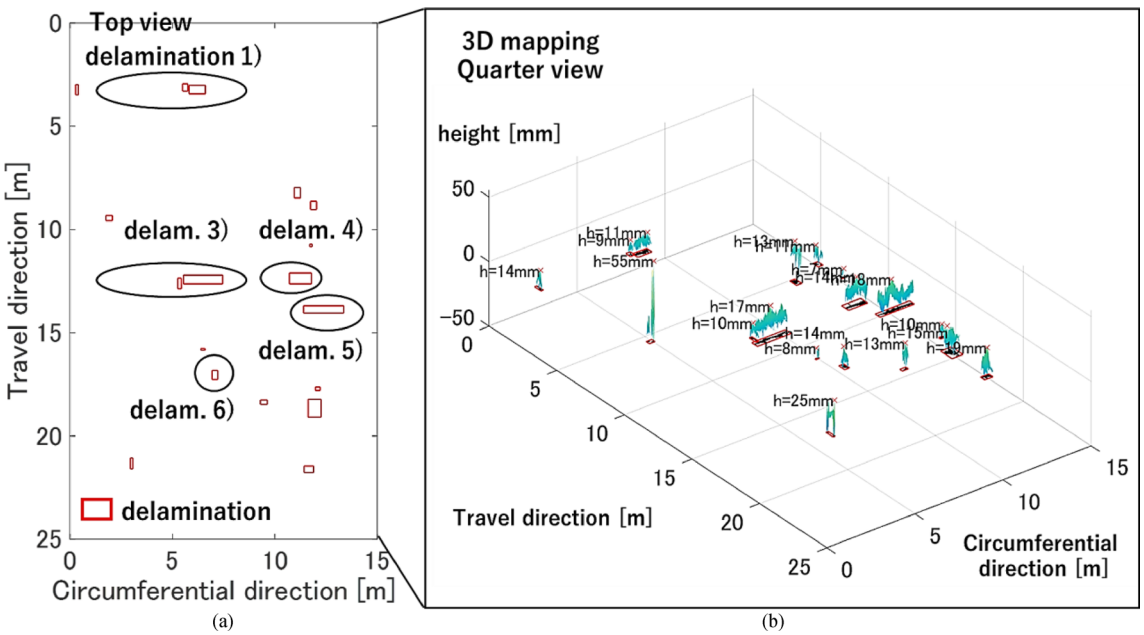

Fig. 10 Detection results of the delamination of the data No. 1 (**a**) Top view of the 3D mapping result, corresponding to a delamination map. **b** Quarter view, showing the 3D shapes of the anomalies. Red cross points represent the highest positions in the detected areas with the estimated maximum heights

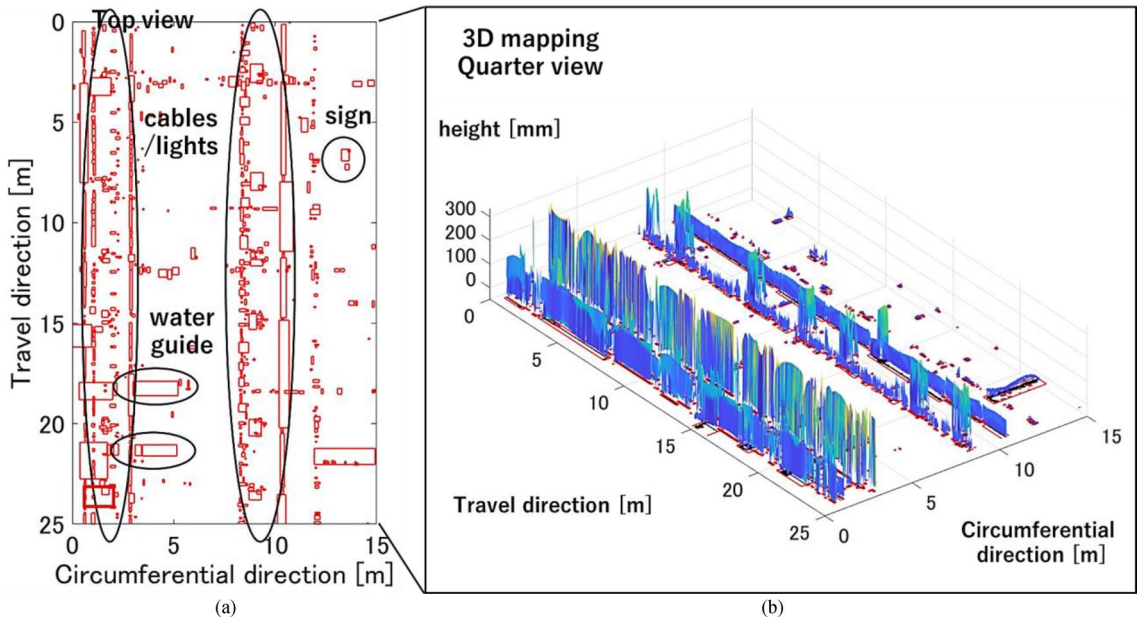

Fig. 11 Detection results of the appendages, which are the remaining areas of the delamination detection results of Fig. 10. **a** Appendage map. **b** Quarter view of the 3D mapping result

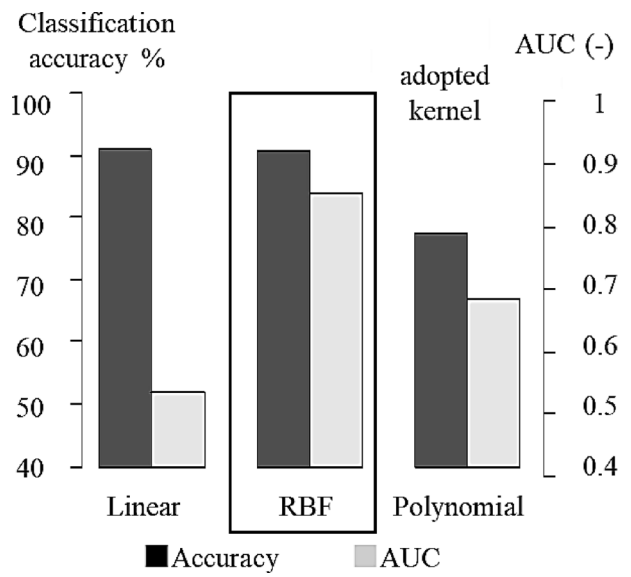

Fig. 12 Effect of the kernel functions on classification accuracy (black) and AUC (gray). Linear is no kernel. Polynomial is third order

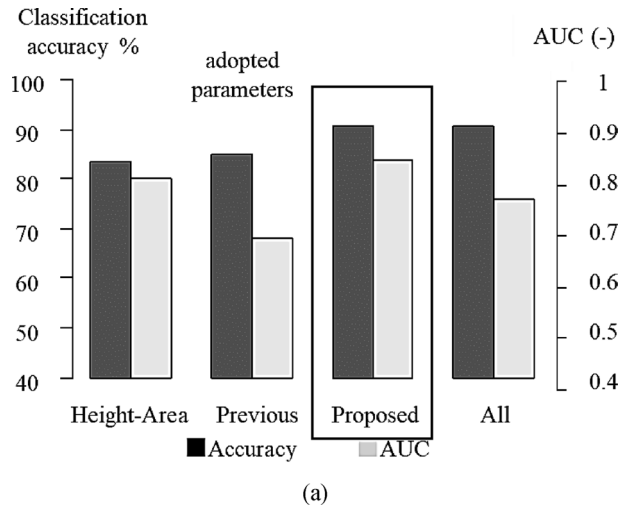

Fig. 13 Effect of the feature parameters on accuracy and AUC

Table 3 Combination of the used feature values for each SVM model

SVM model	Used features
No. 1 (height-area)	(h, s)
No. 2 (previous)	$(h, s, O_{yz}, O_{zx}, O_{xy})$
No. 3 (proposed)	$(h, s, O_{yz}, O_{zx}, O_{xy}, S_{yz})$
No. 4 (all)	$(h, s, O_{yz}, O_{zx}, O_{xy}, S_{yz}, S_{zx}, S_{xy})$

has not been systematically compared in the previous studies. Figure 13 compares the accuracy and AUC. The larger the number of the feature parameters was, the higher the accuracy was. The most accurate SVM model was developed considering size, occupancy, and straightness. The accuracy of the proposed model was improved by approximately 6% compared to that of the previous model. However, the proposed models with all the feature values show the same accuracy. The straightness in the horizontal plane can accurately evaluate the straight lines of the profiles. The highest AUC was achieved by the proposed model. Figure 14

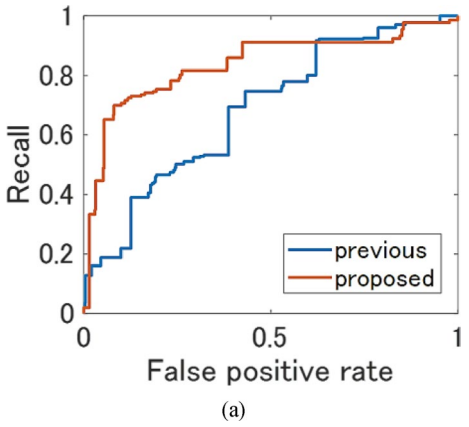

(a)

Fig. 14 Comparison of the PR curves of the previous (blue) and proposed (red) SVM models

shows precision–recall (PR) curves. Recall is the ratio of the number of the detected delamination among all the delamination. False-positive rate is the ratio of the number of the false detection among all the detected possible delamination. Recall and false-positive rate define the axes of the ordinate and abscissa of the PR curves. AUC is the area under the curves. Figure 14 indicates that the AUC was improved by adding a new feature, straightness.

The probability of delamination p is fitted to each feature vector, the threshold of which is the only tuning parameter of the proposed detection algorithm based on the SVM. Figure 15 compares the delamination maps of Fig. 10a changing the minimum probability, P ($p > P$) from 0.1 to 0.9. Figure 10a is the case $P = 0.5$. Figure 15 includes the delamination with various heights and areas in a 25 m section. The optimized P has a certain validity. From Fig. 15a, the entire delamination was successfully detected, while the false detection cases increased in the case of $P = 0.1$. On the other hand, from Fig. 15c, a few areas of the delamination were missing in the case of $P = 0.9$. $P = 0.5$ is optimal from Fig. 15b. In a practical sense, there is a tradeoff between false detection and missing delamination cases. A smaller P indicates a safer side evaluation; a larger P is vice versa. Missing delamination areas may not be favorable. In that case, a smaller P is appropriate.

7 Discussions

A completely automatic algorithm for detecting the delamination on tunnel concrete lining surfaces based on an SVM was proposed. The contribution of this research compared with other research is that the automatic algorithm for detecting delamination from tunnel lining laser profile data is first proposed. Because real tunnels are considered, appendages are distinguished from delamination by the SVM reducing false detection cases.

From the results of Fig. 10, after adopting an appropriate kernel function, proposed feature values, and moderate probability threshold, a high-accuracy SVM algorithm was developed and validated by the real tunnel test data. Appendages such as cables and lights were also successfully visualized. The large delamination such as delamination No.2 and smaller appendages around cables were confused by the algorithm. Future work for the improvement of the algorithm and practical limitations is discussed below.

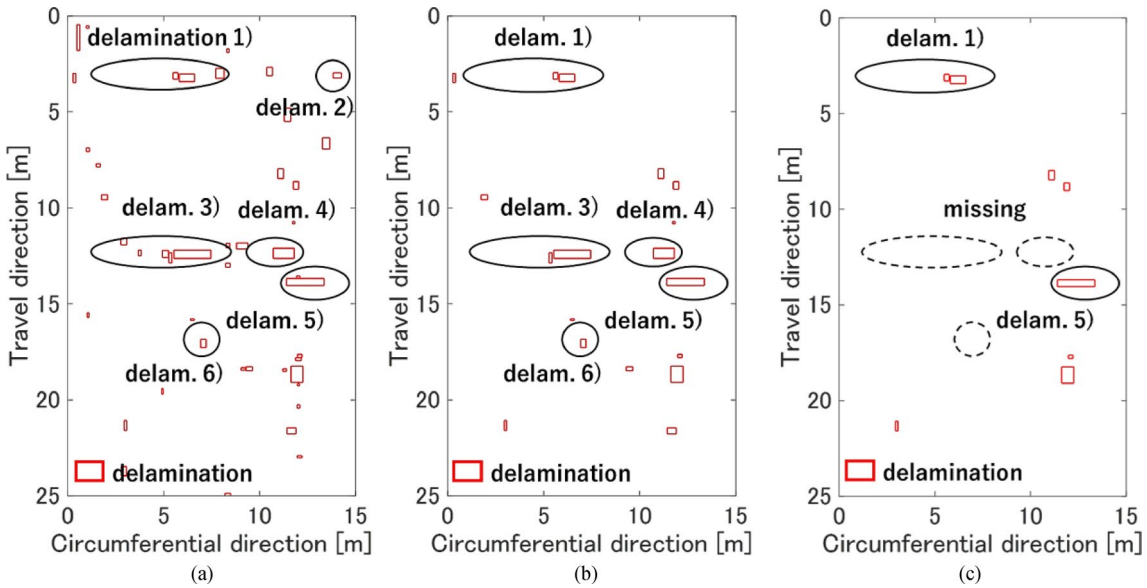

(a) (b) (c)

Fig. 15 Delamination maps of the optimized SVM model with the different probability thresholds P. **a** $P = 0.1$. **b** $P = 0.5$. **c** $P = 0.9$

- The resolution of laser data is crucial for accurate detection. The resolution was set to 2 cm. The speed of the measurement vehicle was 10–20 km/h to obtain the 2 cm resolution. Increasing the speed lowered the resolution. The required resolution depends on the characteristics of the target features. The optimization of the measurement conditions may be needed to realize the further high-speed measurements. The utilization of repeatedly measured data is considered though it is difficult because of the data-matching problem. Considering laser luminance data and optical camera images may increase accuracy. The estimation accuracy of the 3D shapes of delamination was not discussed because of the complicated and ambiguous shapes of the real delamination. The utilization of artificial delamination models and simulation data may improve the classification accuracy of the algorithm.

Different tunnel data were prepared for the SVM training and validation. Therefore, the algorithm can be applied to other tunnel datasets. However, because of the characteristics of a mobile mapping system (MMS), which is a vehicle equipped with laser scanning sensors, target tunnels are mainly highway road tunnels. The developed algorithm may be applicable to railway tunnels.

8 Conclusions

An automatic and accurate SVM algorithm for detecting delamination on tunnel concrete lining surfaces using laser 3D point cloud data was developed. The algorithm consists of two steps: extraction of 3D shapes and detection of delamination by SVM. The second step was developed in this study to achieve accurate and automatic detection. The introduction of straightness and automatic detection by an SVM are the contributions. Artificial objects such as cables and lights were characterized by defining the straightness of feature profiles. The SVM was trained and validated using the data of real tunnel concrete lining surfaces. A parametric study was conducted to optimize the model parameters and determine the most appropriate probability threshold. Including straightness improved accuracy by 6% and AUC by 0.3 compared with the previous model. The proposed algorithm successfully visualized the areas of the delamination on a map with their realistic 3D shapes, enabling automatic and high-speed tunnel lining inspection.

In future work, the algorithm can also be applied to the detection of peeling on concrete surfaces and road potholes. Delamination on concrete walls of other types of infrastructures is also a possible application. The validation data was limited to the highway road tunnels. The developed algorithm may be applied to railway tunnels and other large-scale data to conduct regional and time-series analysis of aging tunnels. The estimation of the tunnel cross sections from the infrastructure profiles in the step 1.1 is also considered to monitor tunnel deformations. There is a limitation in the vehicle speed. Measuring the same tunnel multiple times and considering laser luminance data and camera images may further improve the performance. The optimization of the measurement conditions remains as a topic for future work.

Funding Open access funding provided by The University of Tokyo. This research was supported by Ministry of Land, Infrastructure, Transport and Tourism (MLIT) "Research and development that contributes to improving the quality of road policies" program (New CART COMMITTEE ON ADVANCED ROAD TECHNOLOGY) (Grant No. 31-6).

Data availability The authors do not have a permission to provide the measurement data shown in this article.

References

1. American Society of Civil Engineers (ASCE) (2022) Infrastructure report card, USA. [Online]. https://infrastructurereportcard.org/. Accessed 8 May 2022
2. Ministry of Land, Infrastructure, Transport and Tourism (2022) Statistics about roads, (in Japanese), Japan. [Online]. https://www.mlit.go.jp/road/soudan/soudan_10.html. Accessed 8 May 2022
3. Ministry of Land, Infrastructure, Transport and Tourism (2022) Road tunnel regular inspection manual, (in Japanese), Japan. [Online]. https://www.mlit.go.jp/road/sisaku/yobohozen/tenken/yobo3_1_9.pdf. Accessed 8 May 2022
4. Omar T, Nehdi ML (2017) Remote sensing of concrete bridge decks using unmanned aerial vehicle infrared thermography. Autom Constr 83:360–371
5. Blaney S, Gupta R (2018) Sounding of subsurface concrete defects using frequency response of flexural vibration. Cem Concr Compos 92:155–164
6. Yasuda N, Misaki N, Shimada Y, Yamaoka D (2020) Detection and characteristics estimation of defects in concrete structures using laser ablation-induced vibration. Tunn Undergr Space Technol 103:103460
7. Otake Y (2019) Non-destructive infrastructure testing by compact neuron source. IEEJ J 139(5):296–299
8. Yamaguchi T, Mizutani T, Tarumi M, Su D (2019) Sensitive damage detection of reinforced concrete bridge slab by "time-variant deconvolution" of SHF-band radar signal. Inst Electr Electr Eng Trans Geosci Remote Sens 57(3):1478–1488
9. Aero Asahi Corporation (2022) Roads: mobile mapping system (in Japanese), Japan. [Online]. https://www.aeroasahi.co.jp/spatialinfo/social_infra/road/. Accessed 8 May 2022

10. Kim MK, Cheng JCP, Sohn H, Chang CC (2015) A framework for dimensional and surface quality assessment of precast concrete elements using BIM and 3D laser scanning. Autom Constr 49:225–238
11. Yoon JS, Sagong M, Lee JS, Lee KS (2009) Feature extraction of a concrete tunnel liner from 3D laser scanning data. NDT&E Int 42:97–105
12. Mizutani T, Yamaguchi T, Kudo T, Yamamoto K, Ishida T, Nagata Y, Kawamura H, Tokuno T, Suzuki K, Yamaguchi Y (2022) Quantitative evaluation of peeling and delamination on infrastructure surfaces by laser signal and image processing of 3D point cloud data. Autom Constr 133:104023
13. Yamaguchi T, Mizutani T, Kudo T, Yamamoto K, Ishida T, Nagata Y, Kawamura H, Tokuno T, Suzuki K, Yamaguchi Y (2022) Detection of delamination and peeling on infrastructure surfaces by time-series analysis and 3D feature extraction of laser 3D point cloud data. J Japan Soc Civ Eng Ser F1 78(1):112–131
14. Goodfellow I, Bengio Y, Courville A (2016) Deep learning, 1st edn. The MIT Press, Cambridge
15. Simonyan K, Zisserman A (2015) Very deep convolutional networks for large-scale image recognition. In: International conference on learning representations, California
16. Szegedy C, Liu W, Jia Y, Sermanet P, Reed S, Anguelov D, Erhan D, Vanhoucke V, Rabinovich A (2015) Going deeper with convolutions. In: Institute of electrical and electronics engineers conference on computer vision and pattern recognition, Massachusetts
17. Bishop CM (2006) Pattern recognition and machine learning, 1st edn. Springer, Berlin
18. Llorca DF, Arroyo R, Sotelo MA (2013) Vehicle logo recognition in traffic images using HOG features and SVM. In: Institute of electrical and electronics engineers international conference on intelligent transportation systems, Hague
19. Shao Y, Lunetta RS (2012) Comparison of support vector machine, neural network, and CART algorithms for the land-cover classification using limited training data points. J Photogramm Remote Sens 70:78–87
20. Chatzis MN, Chatzi EN, Smyth AW (2014) An experimental validation of time domain system identification methods with fusion of heterogeneous data. Earthq Eng Struct Dyn 44(4):523–547
21. Oppenheim AV, Schafer RW (2010) Discrete-time signal processing, 3rd edn. Pearson, London
22. Cohen L (1995) Time-frequency analysis, 1st edn. Prentice Hall, New Jersey
23. Peters RA (1995) A new algorithm for image noise reduction using mathematical morphology. Inst Electr Electr Eng Trans Image Process 4(5):554–568
24. Haralick RM, Sterberg SR, Zhuang X (1987) Image analysis using mathematical morphology. Inst Electr Electr Eng Trans Pattern Anal Mach Intell PAMI-9(4):532–550
25. Hirano H, Mizutani T, Ishida T, Annaka S, Suzuki K (2018) Evaluation of local deterioration of pavement surface by spatial frequency analysis based on short-time Fourier transform. Jpn J Pavement Eng 74(3):I-113–I–120
26. Lobo JM, Jimenez-Valverde A, Real R (2007) AUC: a misleading measure of the performance of predictive distribution model. Glob Ecol Biogeogr 17:145–151
27. Ren S, He K, Girshick R, Sun J (2017) Faster R-CNN: towards real-time object detection with region proposal networks. Inst Electr Electron Eng Trans Pattern Anal Mach Intell 39(6):1137–1149
28. Liu W, Anguelov D, Erhan D, Szegedy C, Reed S, Fu CY, Berg AC (2016) SSD: single shot multibox detector. In: European conference on computer vision, Amsterdam
29. Redmon J, Divvala S, Girshick R, Farhadi A (2016) You only look once: unified, real-time object detection. In: Institute of electrical and electronics engineers conference on computer vision and pattern recognition, Nevada